# Annual performance of subcritical Rankine cycle coupled to an innovative particle receiver solar power plant

**Article** *in* Renewable Energy · January 2019

DOI: 10.1016/j.renene.2018.06.109



Miguel ANGEL Reyes Belmonte
Madrid Institute for Advanced Studies


Andrés Sebastián
Universidad Politécnica de Madrid


Marianna Romero
Hospital Universitario de Caracas

Renewable Energy 130 (2019) 786–795

Contents lists available at ScienceDirect

Renewable Energy

journal homepage: www.elsevier.com/locate/renene

# Annual performance of subcritical Rankine cycle coupled to an innovative particle receiver solar power plant

M.A. Reyes-Belmonte, A. Sebastián, J. Spelling, M. Romero*, J. González-Aguilar

*IMDEA Energy Institute, Avda. Ramón de la Sagra, 3, 28935, Móstoles, Madrid Spain*

A R T I C L E I N F O

*Article history:*
Received 28 February 2018
Accepted 29 June 2018
Available online 29 June 2018

*Keywords:*
Solar thermal
Steam Rankine cycle
Thermodynamics optimization
Particle receiver

A B S T R A C T

Concentrated solar power plants using molten salts as heat transfer and storage fluid have emerged as the preferred commercial solution for solar thermal electricity in central receiver technology. Despite their ability to store large amounts of thermal energy and efficient receiver designs, further efficiency improvements are constrained by tight temperature restrictions when using molten salts (290 °C −565 °C). In this work, a novel heat transfer fluid based on a dense particle suspension (DPS) is used due to its excellent thermophysical properties that extend the operating temperature of solar receiver and allow its coupling with higher-efficiency power cycles. In this paper, the design of a DPS solar receiver working at 650 °C has been optimized for two commercial sizes (50 $MW_{th}$ and 290 $MW_{th}$) coupled to an optimized subcritical Rankine cycle. The results showed that a five-extraction reheated Rankine cycle operating at 610 °C and 180 bar maximizes power plant efficiency when coupled with a DPS central receiver, giving 41% power block efficiency and 23% sun-to-electricity efficiency. For optimization purposes at design point conditions, in-house code programmed into MATLAB platform was used while TRNSYS software was employed for annual plant performance analysis.



## 1. Introduction

The installation and use of renewable energy sources for electricity production is gaining in importance due to stringent environmental standards seeking to reduce pollutant emissions and fossil fuel dependence. In this context, concentrating solar thermal technologies are considered to be one of the most promising means for electricity production in coming decades [1]. Concentrating solar power (CSP) has shown many advantages compared to other intermittent renewable electricity sources such as wind and photovoltaics. Amongst the main advantages are that solar thermal electricity is reliable, flexible and, when integrated with thermal energy storage (TES) systems, is not limited to operating only when the sun is shining [2]. In addition, when coupled with dry-cooling, the water requirement of CSP technologies is limited [3]. However, cost reductions achieved by competing technologies are forcing CSP developers to move a step further seeking for cost reductions due a highly competitive market and the lack of tariffs that correctly value the dispatchability of CSP [4]. This could be achieved through economies of scale [5,6], by implementing new technological developments leading to higher solar-to-electricity efficiencies and by optimizing operation and maintenance strategies on CSP plants [7,8]. One alternative to increase the efficiency of CSP plants involves using a new heat transfer fluid (HTF) capable of operating at higher temperatures than current direct steam generation or molten salt technologies. Higher temperatures will allow using advanced and highly efficient power cycles such as supercritical $CO_2$ or Combined Cycles which will contribute towards driving down costs of electricity generation [9–12]. One interesting option is the use of a dense gas-particle suspension (or DPS), consisting of very small particles which can be easily fluidized at low gas speeds. The fraction of particles within the suspension is high (up to around 40% by volume [13]) resulting in a fluid with a high density (above 1000 $kg/m^3$) and a significant improvement in heat transfer between the solar collector and the HTF (above 500 $W/m^2K$ [14]). If ceramic particles are considered, extremely high temperatures can be achieved (above 1000 °C [15]), being limited only by the thermomechanical characteristics of the absorber tubes. Furthermore, due to the high particle density, and the ease of separating the particles from the entraining gas flow, TES can be easily implemented through simple bulk storage of hot particles. As the particles remain solid there is no lower temperature limit (as in the case for molten

* Corresponding author.
*E-mail address:* manuel.romero@imdea.org (M. Romero).

https://doi.org/10.1016/j.renene.2018.06.109
0960-1481/

salts), allowing the TES units to operate across a wider temperature range.

With a view to establishing utility scale power plant designs based around this novel HTF, a unified and consistent methodology must be established to design, analyze and optimize power plant components. The central receiver is based on a fluidized bed of particles (type A particles according to Geldart classification [16]) moving upwards through a tubular receiver using air as the entraining gas. Experiments performed on a 150 $kW_{th}$ lab demonstrator at CNRS-PROMES, France, have proved the feasibility of this concept for solar receiver applications [14]. Temperatures up to 650 °C have been experimentally tested opening up the possibility to connect this type of solar receiver to a wide selection of power cycles [17].

Annual performance simulations can be often found in literature as a helpful tool in order to assess the overall yearly behavior of solar power plants. For instance, several works from literature have analyzed the annual performance of innovative solar power plants such as [18] for solar tower aided coal-fired power generation system [10], for solar-hybrid Combined (air receiver and particles receiver) [19], for innovative gas turbine cycles (such as isothermal compression or with ORC as bottoming cycle) [20], for integrated solar combined cycles using different CSP technologies (parabolic trough, Fresnel and Central receiver) or [21] for solar hybrid steam injection gas turbine. However, no previous research works have been found on the optimization and annual performance of Rankine cycles coupled to particles receivers and in particular to upward bubbling fluidized bed that is presented into this paper.

The aim of this paper is to design and optimize a CSP plant using DPS as both the HTF and the TES medium coupled with a high performance Rankine cycle for electricity production; both design-point conditions and annual plant performance will be analyzed. Two different scenarios will be analyzed, firstly a medium scale demonstrator with a 57 $MW_{th}$ receiver, followed by a larger 290 $MW_{th}$ receiver for a larger utility-scale plant. The analysis will be limited to subcritical Rankine power blocks due to the high maturity of these and the well-understood operating behavior that they exhibit in CSP plants.

## 2. Solar power plant description

Fig. 1 shows the layout of the DPS-based central receiver solar power plant using a water/steam Rankine cycle. The main components of the power plant are the heliostat field, the central particle receiver, the hot and cold particles storage tanks, the turbine island, and a series of heat exchangers allowing the thermal energy of the receiver HTF (the DPS) to be passed to the cycle working fluid (water/steam). Silicon Carbide particles have been considered for the solar loop with the material properties shown in Table 1 [22].

The boundary conditions and general specifications of the CSP plant design are presented in Table 2; these were agreed under the framework of the European research project CSP2 [23] where receiver outlet temperatures of 650 °C was achieved [24,25]. For the TES, a solar multiple of 2 with 6 h of storage capacity were the chosen parameters.

## 3. Methodology

The design methodology followed in this paper determines the boundary conditions and sizes of the solar plant components for optimum plant performance. For sizing and optimization purposes, mathematical models of each plant component have been encoded in a MATLAB platform [26, 27]. The optimized design and plant specifications are later translated to the TRNSYS platform [28] for flow sheeting generation and annual performance analysis. TRNSYS has been chosen over other dynamic software due to its flexible simulation environment able to model different transient and dynamic systems, its shorter computational times, its capability to be integrated with MATLAB, the existence of solar components from the STEC library [29] and the ability to create new components or modify existing ones. The WinDelsol software [30] has also been used for optimum heliostat field design; the software interactions are shown on Fig. 2.

Meteorological data (typical meteorological year with 10 min resolution) was used to determine the thermal input from the solar field, based on the direct normal irradiance (DNI) and the Sun's position. In addition, a detailed control and operation strategy was defined within TRNSYS to address plant start-ups, storage management and receiver thermal control.

### 3.1. Steady-state design

Component design optimization under steady state (or nominal

**Table 1**
Silicon carbide particles properties.

| Property | Units | Value |
|---|---|---|
| Sauter mean diameter | [μm] | 63.9 |
| Density | [kg $m^{-3}$] | 3210 |
| Specific heat capacity (at 500 °C) | [J $kg^{-1}$ $K^{-1}$] | 1150 |
| Thermal conductivity (at 500 °C) | [W $m^{-1}$ $K^{-1}$] | 109 |

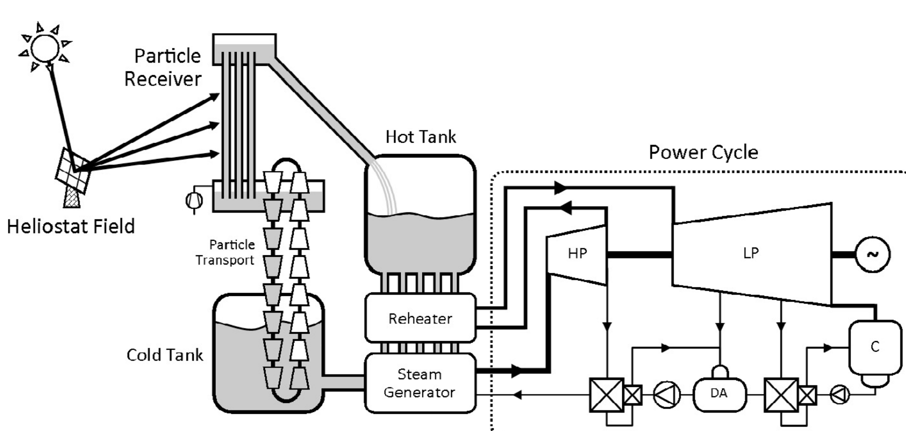


**Fig. 1.** Concentrating solar power plant layout [50] .

**Table 2**
CSP plant design specifications.

| Specification | Value |
|---|---|
| Nominal Thermal Power at Receiver | 57 $MW_{th}$<br>290 $MW_{th}$ |
| Receiver Outlet Temperature | 650 °C |
| Solar Multiple | 2 |
| Storage Capacity | 6 h |
| Power Block | Reheated Rankine |
| Nominal Ambient Temperature | 30 °C |
| Suggested Power Plant Location | Ouarzazate, Morocco<br>30.9°N, 6.93°W |
| Design point | Spring Equinox - Noon |

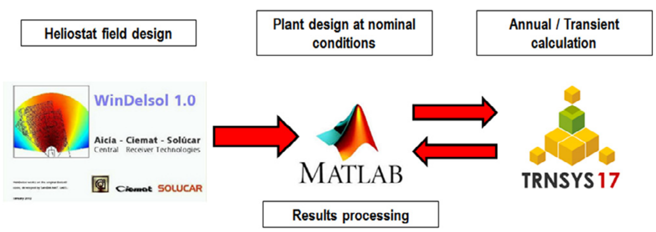


**Fig. 2.** Proposed modelling procedure.

conditions) is addressed in a backward direction, starting from the desired electricity output of the power block as is shown in Fig. 3. Electrical power output sets the boundary condition for optimization of the power block (based on maximizing the efficiency of energy conversion) and determines the required thermal input power. The required thermal energy from the heat transfer fluid loop is then determined based on the heat exchangers efficiency connecting the solar loop with the power cycle. This is then increased by the solar multiple to give the required absorbed thermal energy on the receiver. Once thermal losses from the receiver are accounted for (mainly radiation and convection losses), the energy reaching the receiver is determined and used as the basis for the heliostat field design. The solar-to-electricity efficiency of the plant ($\eta_{total}$) is obtained considering all the efficiencies involved in the energy balance problem as shown by equation (1).

$$\eta_{total} = \eta_{hel} \cdot \eta_{rec} \cdot \eta_{HTX} \cdot \eta_{cycle} \tag{1}$$

Where $\eta_{cycle}$ represents power cycle net efficiency and has been defined as the net electric output of the power cycle divided by the thermal input power to the cycle. Term $\eta_{HTX}$ represents the efficiency of the heat exchanger that is connecting the solar loop and the power loop [31]. It has been defined as the ratio between the thermal power transferred to the working fluid of the power cycle and thermal power of the particles. Parameter $\eta_{rec}$ represents thermal efficiency of particles solar receiver and it is defined as the ratio between the useful heat transferred to dense particle suspension (DPS) and the incident power reaching the receiver. Finally parameter $\eta_{hel}$ represents the efficiency of the solar field and it is defined as solar incident power reaching the heliostat field and reflected power reaching solar receiver.

### 3.2. Solar field

For heliostat field design optimization, the WinDelsol software [30] (based on the original Delsol3 [32] developed by SANDIA National Labs) has been used. In order to accelerate the calculation of large heliostat fields, a cell-wise approach was adopted. Doing so, the land is divided into a number of "cells" within which it is assumed that all heliostats perform identically. As such, the power delivered to the central receiver by a given cell is determined by multiplying the output from a representative heliostat located at the centre of the cell by the number of heliostats within the cell. The number of heliostats within each cell is a function of the local heliostat field density, $\rho_{cell}$, which is the ratio of mirror area to land area. As the distance between the heliostats and the central tower increases, the field density decreases, as a greater amount of space needs to be left between adjacent heliostats in order to prevent shadowing and blocking. The thermal power delivered to the receiver by the heliostat field can be calculated by summing the power output of each cell using as indicated by equation (2).

$$\dot{Q}^{-}_{field} = \sum_{cells} \rho_{cell} \frac{A_{cell}}{A_H} \dot{Q}^{-}_H \tag{2}$$

where $A_{cell}$ is the land area within a given cell, $A_H$ is the surface area and $Q_H$ are the power output of the representative heliostat.

Power delivered to the receiver by the representative heliostat within each cell can be calculated using equation (3), based on its surface area $A_H$, the incident solar beam irradiation $I_b$, as well as a number of efficiency and losses factors, $\varepsilon$ and $f$, respectively. From Sun to receiver, they are cosine efficiency ($\varepsilon_{cos}$), mirror reflectance and soiling ($\varepsilon_{surf}$), shadowing and blocking losses ($f_{sb}$ ), atmospheric attenuation ($f_{att}$) and finally interception losses, or spillage ($f_{spill}$).

$$\dot{Q}^{-}_H = A_H I_b \cdot \varepsilon_{cos} \varepsilon_{surf} \cdot (1 - f_{sb})(1 - f_{att})\left(1 - f_{spill}\right) \tag{3}$$

Once the layout of the heliostat field has been determined for a given design thermal power, its performance (efficiency and thermal power output) will solely depend upon the intensity of the DNI and the position of Sun in the sky. As such, inclusion of the heliostat field operation in simulation is greatly simplified by the use of a field efficiency matrix, which maps the overall heliostat field efficiency as a function of the solar position (azimuth and elevation). To sum up, results obtained from heliostat field optimization process are the efficiency matrix, the tower height, the number of heliostats and their area. All these parameters will be assigned to the MATLAB routines as input parameters. The global optimized efficiency matrix of the solar field takes into account the cosine efficiency, heliostats blocking and shadowing effects, spillage and ambient attenuation.

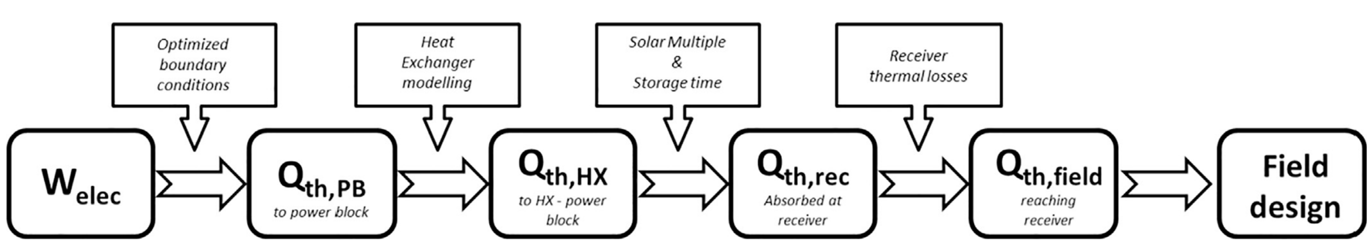


**Fig. 3.** Flowchart of the CSP plant design methodology.

### 3.3. Particle suspension receiver

An overview of the considered solar particle receiver concept is shown in Fig. 4, cold particles are taken from a storage hopper and conveyed to an air-driven fluidized bed. The fluidized particles pass up through the tubes of the absorber, onto which the concentrated solar radiation is focused, heating the particles up to the desired temperature.

A unique characteristic of the system considered, is the use of very small particles which require low fluidization speeds and occupy a relatively large volume fraction (up to 40%) of the fluidized suspension. Particle suspensions have a relatively large density, similar to that of a liquid, increasing the quantity of heat that can be absorbed by a given volume of flow and the particulate nature of the flow allows high heat transfer coefficients to be reached. The low fluidization speed also serves to minimise the gas flowrate, reducing blower auxiliary power, as well as component abrasion and particle attrition.

According to the simplified particles receiver model presented by Gallo et al. [33], the required particles mass flow ($\dot{m}_p$) can be determined from receiver energy balance equation (4).

$$\dot{m}_p = \frac{\dot{Q}_{th,rec}}{c_{p,p}\left(T_p^{out} - T_p^{in}\right)} \tag{4}$$

Where DPS inlet and outlet temperatures are assumed at design stage, while the absorbed thermal power inside the receiver will be initially estimated prior determination of receiver thermal losses.

In order to drive the flow of particles through the receiver tubes, a mass flow of gas ($\dot{m}_g$) is required, which can be calculated based on the particle volume fraction ($\phi_p$), particle and gas velocities ($u_g$) and the DPS characteristics as shown by equation (5). This gas mass flow, whilst absorbing heat during passage through the receiver, does not have its energy harnessed, and will constitute an additional source of thermal losses.

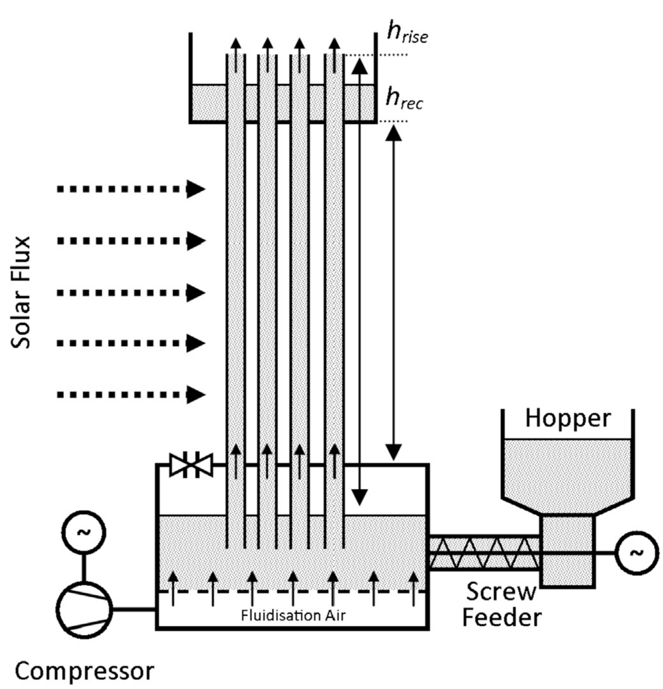


**Fig. 4.** Schematic illustration of the dense particle receiver concept [14].

$$\dot{m}_g = \frac{(1-\varphi_p)\rho_g u_g}{\varphi_p \rho_p \left(u_g - u_{mf}\right)} \cdot \dot{m}_p \tag{5}$$

The total mass flow of the suspension through the receiver ($\dot{m}_{DPS}$) is then defined as the sum of these two flows ($\dot{m}_p$and $\dot{m}_g$).

Once the physical properties of DPS have been established, global heat transfer analysis of the absorber tubes can be performed with a view to determining the required geometric characteristics of the receiver setup. As was pointed out by Gallo et al. [33], the incident solar radiation will only impact the absorber tubes on one side, resulting in a non-uniform temperature distribution in the metal. A hotter zone will form on the side absorbing the radiation and heat will be conducted away from this zone around the circumference of the tubes, exchanging with the fluid at a lower temperature.

Fin analogy has been applied assuming that no heat is transferred circumferentially at the back of the tubes and the lateral sides of the tubes are considered as two separated fins. Overall heat transfer rate $U$ from the tube to the dense particle suspension can be calculated using equation (6).

$$U = f_{act} \cdot \alpha_{\mathrm{DPS}} + 2\frac{\sqrt{\alpha_{\mathrm{DPS}}\lambda_t t_t}}{\pi\, d_i} \tanh\left[\pi\left(d_i + \frac{t_t}{2}\right)\left(\frac{1-f_{act}}{2}\right)\sqrt{\frac{\alpha_{\mathrm{DPS}}}{\lambda_t t_t}}\right] \tag{6}$$

The internal convective heat transfer coefficient ($\alpha_{DPS}$) can be determined from experimental works [13,17,25]. The total number of tubes ($N_{tubes}$) required in the absorber array is a function of the ratio between the DPS mass flow ($\dot{m}_{DPS}$) and the mass flux of the suspension ($G_{DPS}$), and can be estimated from equation (7).

$$N_{tubes} = \frac{4\dot{m}_{\mathrm{DPS}}}{\pi\, d_i^2 G_{\mathrm{DPS}}} \tag{7}$$

The mass flux of the suspension ($G_{DPS}$) can be determined from equation (8) based on particles properties.

$$G_{\mathrm{DPS}} = \varphi_p \rho_p \left(u_g - u_{mf}\right) + (1-\varphi_p)\rho_g u_g \tag{8}$$

Provided tubes length and diameters are known, the required heat transfer area $A$ will be determined from the number of tubes; after that receiver thermal losses (radiative and convective) can be estimated which will lead to a calculation of the real power absorbed at the receiver [33]. In case the calculated absorbed power does not match with the initially assumptions, the process is repeated from equation (4) until convergence on the number of tubes is reached. Solving this iterative procedure can be seen in Fig. 5.

### 3.4. Solid particle heat exchanger

A heat exchanger (HX) is required to transfer the thermal energy captured by heat transfer fluid (particles suspension) to the power block [34]. Due to the consideration of a power block configuration based on a reheated steam Rankine cycle, a four-stage heat exchanger from the DPS to the water/steam is required. These are the economizer HX for feedwater preheating, the evaporator HX for steam generation, the superheater HX to achieve the required steam conditions (high temperature turbine inlet conditions), and finally the reheater HX to achieve high steam temperature for medium pressure turbine expansion. The heat exchanger connecting the solar loop and the power block is based on fluidized bed technology as it has been proposed by several researchers [35–37]. Detailed modelling of fluidized-bed heat exchanger for subcritical

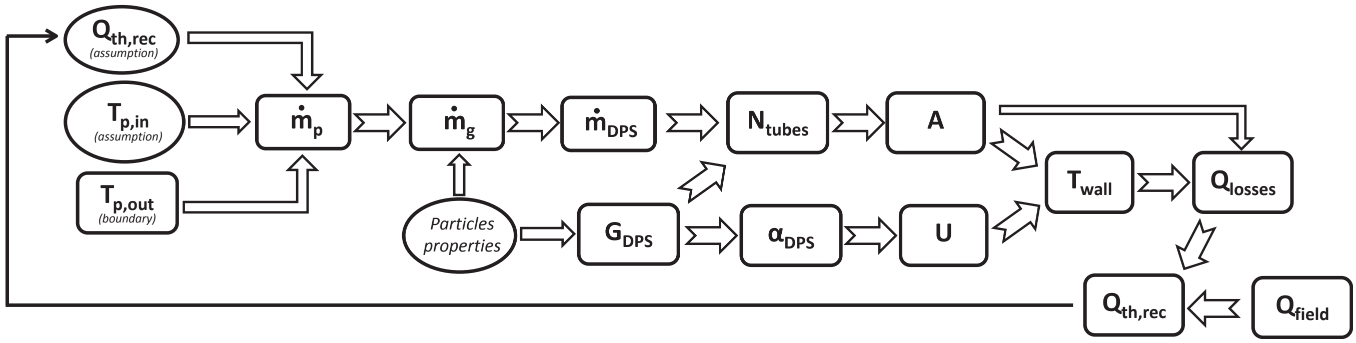


**Fig. 5.** Receiver solving algorithm.

Rankine cycle has shown that its efficiency varies from 93% to 99% [31]. Assuming an average efficiency of 95%, as shown in Table 3 seems a plausible assumption.

### 3.5. Power block

Power cycle boundary conditions are optimized in order to maximize energy conversion efficiency and ensure good quality steam for each turbine stage. Due to the higher temperatures achieved by the DPS receiver, higher steam pressure and temperature than is typical for a CSP Rankine cycle can be obtained. Steam extractions are optimized in order to reduce energy consumption for water preheating and maximize the power cycle efficiency.

Modelling parameters for each component of the solar plant are presented in Table 3, a distinction between input parameters to the different models and the calculated ones has been included. Main assumptions for each model are included as well.

**Table 3**
Modelling parameters for each main component.

| Inputs parameters | Optimization parameters | Assumptions |
|---|---|---|
| **SOLAR FIELD** | | |
| Location | Field efficiency matrix | Given thermal input power reaching the receiver ($Q_{th,field}$) |
| Design point (date, hour) | f (cosine, attenuation, spillage, shadow and blockage) | Max radiation heat flux |
| DNI | Number of heliostats | Aiming point strategy |
| Heliostats area ($A_H$) | Heliostat layout | |
| Surface efficiency ($\varepsilon_{surf}$) | Tower height | |
| **RECEIVER** | | |
| Field power ($Q_{field}$) | DPS mass flow ($m_{DPS}$) | Heat transfer correlation ($h_{conv}$) |
| Tubes geometry (h and d) | Receiver surface area (A) | |
| $T_{OUT,\ DPS}$ | Number of tubes ($N_t$) | |
| Tube thickness | Overall heat transfer coefficient (U) | |
| Tube absorbance | | |
| Tube emittance | Receiver wall temperature ($T_w$) | |
| | Heat losses ($Q_{rad}$ & $Q_{conv}$) | |
| | Receiver absorbed power ($Q_{th,rec}$) | |
| **THERMAL ENERGY STORAGE** | | |
| Receiver absorbed power ($Q_{th,rec}$) | Volume tank | Solar multiple (SM) |
| | Thermal power to the HX ($Q_{th,HX}$) | Storage capacity |
| | Thermal heat losses | |
| **SOLID PARTICLE HEAT EXCHANGER** | | |
| m (DPS) | Number of stages | Design to achieve 95% efficiency |
| m (water) | Number of tubes | Heat transfer correlations ($h_{conv}$) |
| $T_{IN,DPS}$ | Tube pass design | |
| $T_{OUT,\ water}$ | Tubes length | |
| **POWER BLOCK** | | |
| $T_{max}$ (cycle) | m (water) | $T_{min}$ (cycle) |
| $P_{max}$ (cycle) | m (extraction steam) | $\eta_T$ |
| $P_{min}$ (cycle) | P (each stage) | $\Delta p$ |

### 3.6. Annual performance

In order to assess power plant performance under annual operation, a control strategy is required to deal with intermittent weather conditions, power block start-ups and solar resource variations along the time. Control strategy must ensure that the power plant will operate respecting safety limits, especially that the maximum surface receiver temperature is not exceeded. In addition, the control strategy will be tailored for power plant energy harvesting providing a suitable environment for nominal working conditions [38,39]. In order to ensure these working principles, several control strategies on heliostat field, central receiver, storage tanks and steam turbine were adopted.

A defocusing strategy on the heliostat field was implemented in the annual model to limit the thermal power reaching the receiver. In this way, the thermal receiver could be working at design conditions with a slight overrun of 5%. Another control strategy was defined for the central receiver in order to compensate fluctuations of reflected power by the heliostats. As it exposed on equation (4), DPS mass flow depends on the thermal power absorbed in the receiver *($Q_{th,rec}$)*, for this reason mass flow will be controlled to maintain the receiver wall temperature below its safety limit. In addition, a minimum input thermal power threshold of 5% was set as minimum energy required for reactor start-up.

Storage tank control strategy is crucial for plant operation under transient conditions, with several approximations proposed in the literature [2,40], be it for peak power production [41] or for transient weather mitigation [42]. For this work, an approach ensuring nominal working conditions for the turbine island was adopted instead. In this scenario, storage tanks were assumed to be emptied during the early hours of the day for plant start-up. During that time, the power plant will run at on-line conditions as if there was not storage system. Main side effect of this approach will be weather fluctuations at morning hours affecting turbine performance, working it at transient mode. After 11 a.m., it was decided that storage tank will take an active role in the operation strategy and incident solar power fluctuations will be covered using thermal energy stored to work the maximum number of hours at design conditions (full-load). Once the sun is set, power plant will continue operating until the hot tank is at 5% of its capacity. Turbines cold start-ups will be considered once minimum thermal power of 25% nominal-plate is reached. This period will last 30 min and 50% of thermal power will be needed during the warm-up, and will not be transformed into electricity. Warm stand-by situations have been contemplated in the model as well but without extra energy required to maintain this operating condition.

## 4. Results and discussion

The optimized power plant layout developed in TRNSYS 16 for the whole system is presented in Fig. 6. Components from the solar field, particle receiver, storage tanks and power block can be seen on the plant layout as well as those used for control strategies (heliostats defocusing, receiver control, tanks control and turbine control strategies). DPS loop and power block were coupled by means of a series of heat exchangers for particles/water (represented in figure as economizer) and particles/steam heat exchangers (marked as evaporator, superheater and reheater) [31]. Turbines steam extractions at different turbine stages are marked as S-split on the figure.

### 4.1. Steady-state modelling results

Design point calculations for the optimization of DPS central receiver working coupled to Rankine cycle are presented below. The optimization process is constrained by some operational and manufacturing restrictions, as it is the case of receiver maximum temperature or tubes length and diameter that were chosen to ensure fluidization and prevent clogging. Heat exchanger design parameters (tubes length, number of steps, diameter …) were also modelling constraints to ensure 95% efficiency at design point conditions [31]. Two power plant scenarios were considered for optimization design and performance analysis; medium size (57 MWth) north oriented polar field with cavity receiver and large size (290 MWth) surrounding field configuration with external receiver. Receiver input parameters can be found on Table 4. The central receiver has been designed following the procedure described on Fig. 5 using input parameters listed in Table 4. Central receiver design has been optimized to maximize energy harvesting (reducing thermal losses) while ensuring operative restrictions are not breached: the tube wall temperature limit is not exceeded, a good fluidization regime is ensured and the temperatures and input thermal power required by the power block are provided. Optimized design parameters for receiver calculation are shown on Table 5; receiver thermal efficiency has been defined as the ratio between the available thermal energy from the heliostat field and the real power transferred to the DPS. Thermal losses occurring at the central receiver are dependent on its geometry, optical properties, surface temperature and meteorological conditions. However the major contributor to thermal losses in the receiver are radiative losses [43], highlighting the benefit of keeping a low temperature at receiver surface. A receiver efficiency of 82.3% was found for medium size plant at design conditions; the lower efficiency compared to usual values for molten salt receivers (that can exceed 88% efficiency [44]) was due to the higher working temperature but also the lower heat transfer coefficient of the DPS (on the range of 500–1000 W/m$^2$K) compared to molten salts (around 5000 W/m$^2$K) [17].

Power cycle parameters (pressure, temperature and steam extractions) are given in Table 6 and were selected to maximize power block efficiency and ensure good steam quality at any turbine stage. Operation parameters calculated for both power blocks are shown on Table 7. As it can be observed, same power plant conditions (number of extractions, turbine efficiencies and inlet conditions) have been considered for both sizes of power plant. The only difference is the steam mass flow and HTF mass flow (DPS) required to

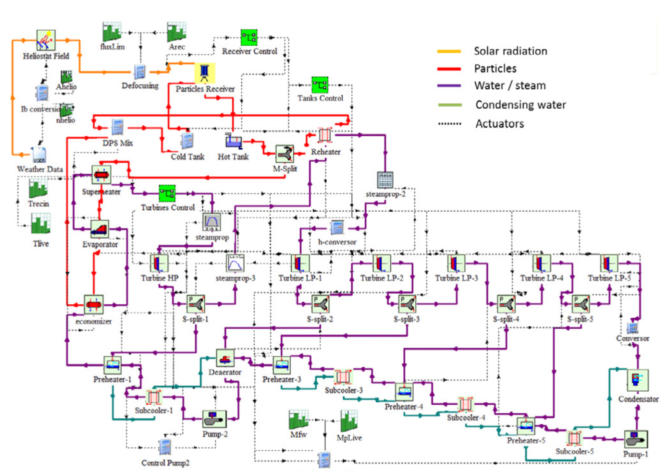


**Fig. 6.** Rankine CSP plant layout generated in TRNSYS.

**Table 4**
Central receiver input parameters.

| Central receiver input parameters | Units | Medium Size | Large Size |
|---|---|---|---|
| Tubes Height | [m] | 8.0 | |
| Tubes Inner Diameter | [mm] | 41.0 | |
| Cavity Opening Angle | [°] | 165 | 360 |
| Input Power from Field | [MW$_{th}$] | 57 | 290 |
| DPS Outlet Temperature | [°C] | 650 | |
| Mean Flux | [kW m$^{-2}$] | 400 | |
| Tower height | [m] | 45 | 175 |

**Table 5**
Central receiver calculated parameters.

| Central receiver optimized parameters | Units | Medium Size | Large Size |
|---|---|---|---|
| Cavity Width | [m] | 12.4 | 28.8 |
| Cavity Radius | [m] | 6.2 | 14.4 |
| Number of Tubes | [#] | 396 | 2015 |
| Absorber Area | [m$^2$] | 143 | 726 |
| Transferred Power | [MW$_{th}$] | 46.8 | 222.1 |
| Thermal Efficiency | [%] | 82.3 | 76.5 |
| Particle Mass Flow | [t h$^{-1}$] | 439.1 | 2081.5 |
| Gas Mass Flow | [kg h$^{-1}$] | 188.9 | 897.4 |

**Table 6**
Power block design conditions.

| Plant Nominal Performance | Units | Medium Size | Large Size |
|---|---|---|---|
| HP Turbine Efficiency | [–] | 0.88 | |
| LP Turbine Efficiency | [–] | 0.91 | |
| Number of Extractions | [#] | 5 | |
| Condenser Type | | Dry | |
| Steam Live Temp. | [°C] | 610 | |
| Reheat Temperature | [°C] | 600 | |
| Inlet HP Pressure | bar | 180 | |

**Table 7**
Power cycle design conditions.

| Plant Nominal Performance | Units | Medium Size | Large Size |
|---|---|---|---|
| Thermal input power | [MW$_{th}$] | 22.1 | 105.1 |
| Heat transfer fluid mass flow | [t h$^{-1}$] | 219.5 | 1040.1 |
| Steam Live Mass Flow | [kg s$^{-1}$] | 7.11 | 33.7 |
| Reheat Pressure | [bar] | 25.0 | |
| Deaerator pressure | [bar] | 14.6 | |

achieve thermal input power.

As it is observed on Fig. 7, two steam turbines have been considered as is the common practice for optimizing subcritical Rankine cycles [45]. High pressure turbine (HP) is expanding the total steam stream (7.11 kg/s) at 610 °C and 180 bar to 341 °C and 25 bar. After this first expansion, a small fraction of the steam is diverted towards the cycle inlet for feedwater preheating meanwhile the main steam stream is reheated at the intermediate pressure of 25 bar. In order to do so, DPS mass flow was divided into two streams, one for the economizer, evaporator and superheater heat exchangers of the cycle and the other for the steam reheater heat exchanger. Mass flow division was calculated in terms of required thermal power for both branches. For design purposes, reheated steam temperature was decided to reach same temperature level that the main steam inlet temperature (610 °C) but assuming extra heat losses leading to input temperature of 600 °C. After that, reheated steam was expanded across an extracting low pressure turbine (LP) where steam was released from various stages of the turbine and sent to boiler feedwater heaters in order to improve overall cycle efficiency [45]. Last turbine stage was connected to the condenser providing vacuum to maximize the energy harvest but also condensing the steam into feedwater to be returned to the boilers. Dry condenser was chosen due to plant location specification being assumed an ambient temperature of 35 °C (design conditions) and a minimum required temperature drop of 15 °C for dry condensing design. At the last expansion, steam was kept at high quality (0.968 as observed in Table 7) to prevent from rapid impingement and blades erosion that will occur when condensed water is blasted onto the blades of the turbine. Exhaust steam conditions were optimized at 50 °C and 0.12 bar, to maximize net cycle efficiency. Standard values for high and low pressure turbine isentropic efficiencies were chosen and the same criterion was followed for piping pressure losses. Plant cycle was completed including water pumps for moving condensed steam and feedwater, both parasitic losses were taken into account for power plant efficiency calculation. Temperature and enthalpy diagrams for the steam process described above can be seen in Fig. 7.

Thermal losses associated with the energy taken by the fluidization air used in the solar receiver and heat exchanger are included in their respective models and considered on power plant overall efficiency. In addition, mechanical power consumption needed for the particles transport system (fan, blowers and screw feeder) have been also estimated according to [33] and taken into account for overall plant efficiency despite, its small effect [46] as it is show on Table 8.

As it is observed on Table 9, heliostat field efficiency for the large size plant was higher than the one obtained for the medium size, based on the better focusing strategy. However thermal losses for the external receiver (large size plant) were higher than the ones found for the cavity receiver (medium size) due to the larger exposed area. For both plant sizes, heat exchangers connecting the solar loop to the power block were designed to ensure 95% efficiency [31]. Due to the fact that the same Rankine cycle power block layout and boundary conditions were considered for both solar plant sizes, no differences appeared on Rankine cycle efficiency. Values found were representative of subcritical Rankine power cycle, while solar-to-electricity efficiency of the proposed plant was around 23% calculated according to equation (1).

**Table 8**
Parasitic losses of the solar plant.

| Plant Nominal Performance | Units | Medium Size | Large Size |
|---|---|---|---|
| Fans and blowers (fluidization air) | [kW] | 4.99 | 23.69 |
| Screw feeder (particles) | [kW] | 6.82 | 32.34 |
| Particles elevation to the tower | [kW] | 82.83 | 152.71 |
| Total parasitic losses | [kW] | 94.64 | 158.31 |

**Table 9**
Receiver plant nominal rate operation.

| Nominal Rate Operation | Efficiency | |
|---|---|---|
| | Medium Size | Large Size |
| Heliostats efficiency | 72.1% | 77.5% |
| Receiver efficiency | 82.3% | 76.5% |
| HX efficiency | 95.0% | 95.0% |
| Net Power cycle efficiency | 40.8% | 40.8% |
| Sun-to-electricity efficiency | 22.99% | 22.97% |
| Net electric production | 9.53 $MW_e$ | 45.1 $MW_e$ |

### 4.2. Annual performance modelling results

Using a yearly based weather data base (Meteonorm [47]) and transient simulation software (TRNSYS) (cf. Section 3), it was possible to reproduce power plant behavior with a 10 min resolution over the whole year. Power plant strategy presented before to account for dynamic modelling can be better understood observing Fig. 8 for two representative days (winter and spring). On the left hand side, modelling results from a typical winter day are shown observing how weather fluctuations before 11 a.m. are affecting turbine performance and electricity production. After that time, turbine will operate at design conditions using thermal energy stored at tanks. It can also be observed that thermal energy at the receiver is below the target of 57 $MW_{th}$ due to the poor solar irradiation at that day and for that reason, heliostats defocusing was not necessary. However, for the spring day shown on the right hand side, thermal energy at the receiver was exceeding 57 $MW_{th}$ target before midday and defocusing strategy was applied that was translated into a flat line at receiver power ($W_{net}$). It was also

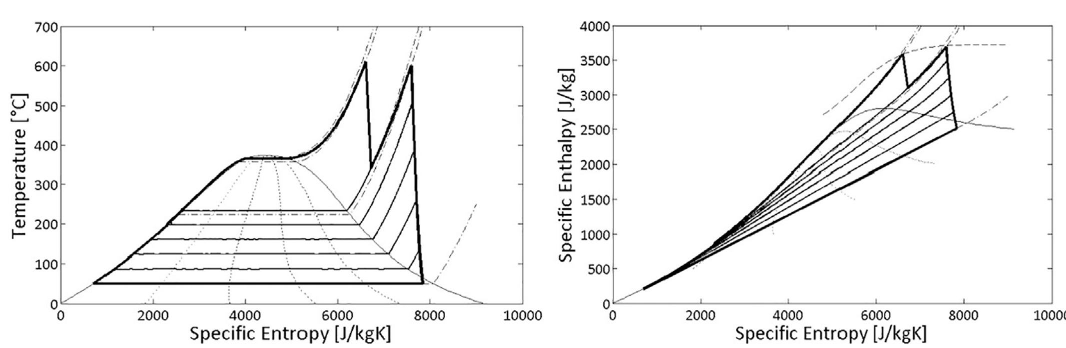


**Fig. 7.** Temperature (left) and enthalpy (right) diagrams for the optimized Rankine cycle.

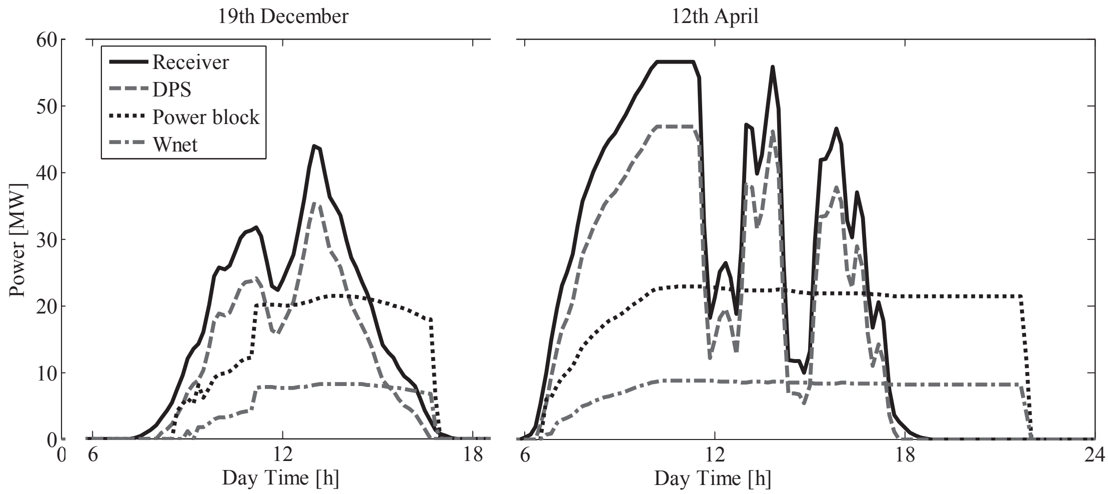


**Fig. 8.** Power plant daily electricity production (medium size case). Left: winter day. Right: summer day.

observed that power block behavior was isolated from any occurring weather fluctuations after 11 a.m. due to thermal energy storage.

Using transient plant strategy observed on Fig. 8; annual heat map shown on Fig. 9 was obtained as a summary of the whole year power plant performance. The figure represented on the x-axis, days of the year, while on the left y-axis the hours of the day were shown and turbine output net power has been displayed with color map being the scale represented on the secondary y-axis (right hand side).

From Fig. 9, whole year power plant performance can be deduced; sunrise, start-ups and shut-downs variations along the year can be easily understood. Integrating that graph, it can be obtained the turbine energy production along the whole year and yearly averaged efficiency for each of the components can be defined as it is shown in Table 10 or in Sankey diagrams for annual energy production (Fig. 10).

As it is observed, major energy losses were found for the solar field (40% for North oriented field and 34% for surrounding field), lower field losses from surrounding field were based on better aiming strategy. However, thermal losses for the external receiver used with surrounding field were higher (17%) than the ones calculated for the cavity receiver off the North field (12%) due to the larger exposed area of the receiver and its bigger size as it was shown on Table 5. As it is observed, lower efficiencies than obtained at design point were expected due to transient variations of the DNI along the year. As it is summarized on Table 10, yearly net power

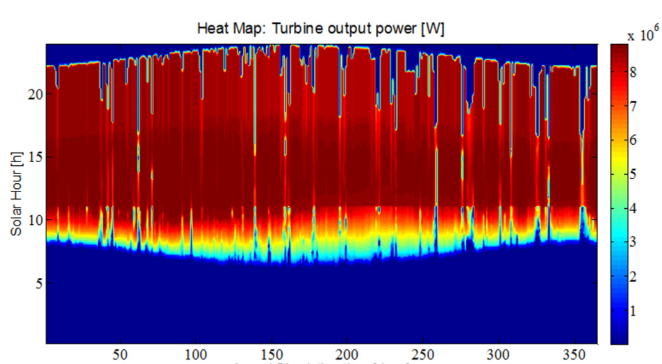


**Fig. 9.** Turbine output power heat map for the medium size plant (57 MWth).

**Table 10**
Central receiver plant annual energy balance.

| Annual Energy Balance | Efficiency | |
|---|---|---|
| | Medium Size | Large Size |
| Heliostats efficiency | 60.1% | 65.5% |
| Receiver efficiency | 78.9% | 73.4% |
| HTX efficiency | 93.4% | 93.4% |
| Net Power cycle efficiency | 37.8% | 37.8% |
| Total annual efficiency | 16.4% | 17.0% |
| Capacity Factor | 55.3% | 55.2% |

cycle efficiency was reduced in three percentage points to 37.8%, meanwhile total annual efficiency of the plant is drastically diminished to 16.4% due to the cumulative effects of power plant components efficiency reduction. Finally, plant capacity factor was around 55% representing the actual power ratio over a period of time, to its potential output if it were possible to operate at full capacity continuously over the same period of time.

## 5. Conclusions

In this paper, an optimization methodology for a central receiver solar power plant has been described and applied to a plant based on a novel dense particle suspension, used as both heat transfer fluid and storage medium. A minimum number of boundary conditions have been set from the project requirements while the rest have been optimized for energy harvesting and efficiency maximizing. The solar receiver using the dense particle suspension was designed and optimized following an iterative solving procedure, considering design restrictions and power plant boundary conditions.

Two thermal power scenarios were considered for power plant components optimization, namely medium and large size solar plants. The heliostat field was designed following an iterative solving procedure to match the receiver's operational requirements with a solar multiple of 2. Storage tanks were designed in order to provide 6 h of storage capacity. A high performance 5-stages reheated subcritical Rankine cycle was optimized for efficiency and coupled to the solar plant using fluidized bed heat exchanger technologies.

Mathematical models were encoded into MATLAB subroutines in order to have a powerful and flexible platform ready to be used

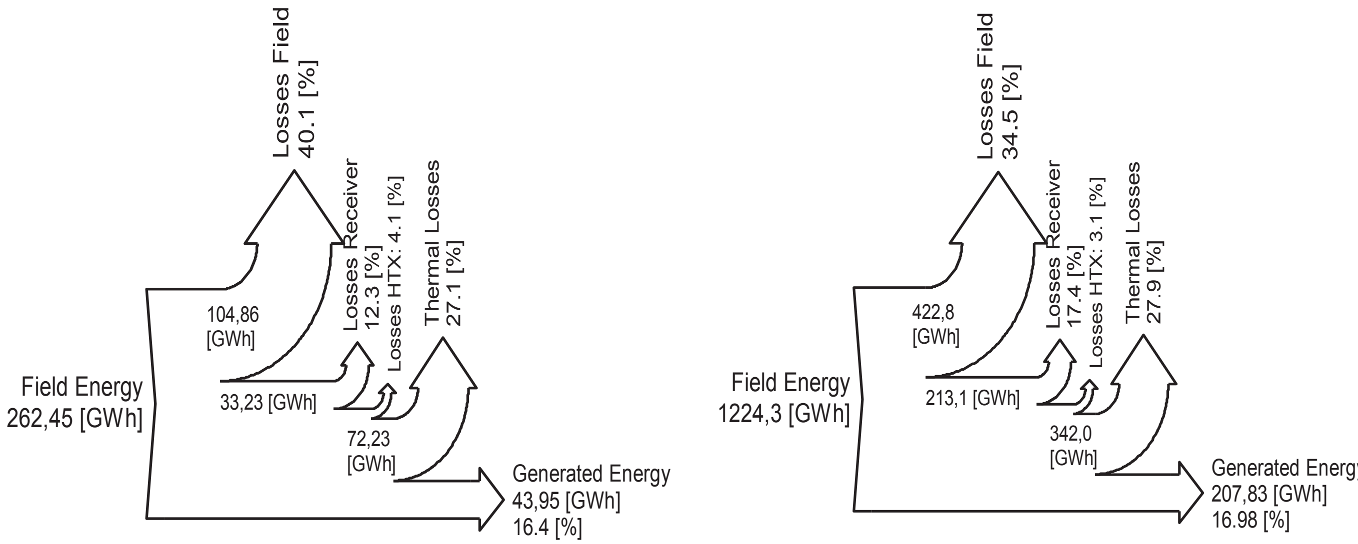


**Fig. 10.** Sankey diagrams of solar plant annual energy production (left: medium size power plant. Right: large size power plant).

for multiple power block configurations or to perform sensitivity studies. Solar power plant performance over a whole year was also analyzed using the TRNSYS platform and proposed a series of control strategies to deal with intermittent weather conditions and power block start-ups in order to assure power block operation under nominal conditions. The power plant working conditions for steady and annual operation agreed with standard practice results from similar plant demonstrators. Optimized solar power plants provided 23% sun-to-electricity efficiency at nominal operation conditions which was reduced down to 17% on an annual basis with 55% capacity factor. Results obtained are showing lower efficiency than state of the art molten salts plant [8]. Despite the higher temperature of the solar receiver (650 °C) that is enabling high temperature Rankine cycle (610 °C) with higher efficiency than current molten salts applications, the overall efficiency (sun-to-electricity) is lower. This is due to the lower thermal efficiency of particles receiver (82%) compared to the typical high values (88%) of molten salts receiver. Nevertheless, particles receiver concept allows for achieving higher temperatures than molten salts receiver (far above 565 °C) which will enable using highly efficient thermodynamic cycles as for example supercritical $CO_2$ cycles and Combined Cycle. Some studies on that area are showing that sun-to-electricity efficiency over 25% can be easily achieved for CSP plants that are using particles receivers in combination with highly efficient power cycles [8,12,48,49].

## Acknowledgements

This study was performed in the framework of the CSP2 Project “Concentrated Solar Power in Particles”, funded by the European Commission (FP7, Project No. 282 932). This project has received funding from the European Union's Horizon 2020 research and innovation programme under grant agreement No 727762, Next-CSP project. The authors would like to thank “Comunidad de Madrid” for its support to the ALCCONES project (S2013/MAE-2985) through the Program of R&D activities between research groups in Technologies 2103, co-financed by structural funds and also thank to the EC for its support through the project EU FP7 IRP STAGE-STE (No. 609837).

## Nomenclature

| | |
|---|---|
| $C_p$ | Specific Heat at Constant Pressure |
| d | Diameter |
| f | Receiver Frontal Area Factor |
| h | Tubes height |
| M | Mass flow |
| Q | Heat |
| T | Temperature |
| u | Velocity |
| U | Overall Heat Transfer Coefficient |

*Abbreviations*

| | |
|---|---|
| CSP | Concentrating Solar Power |
| DNI | Direct Normal Irradiance |
| DPS | Dense Particle Suspension |
| hel | Heliostat field |
| HP | High Pressure Turbine |
| HTF | Heat Transfer Fluid |
| HTX | Heat Exchanger |
| LP | Low Pressure Turbine |
| PV | Photovoltaics |
| rec | Central Receiver |
| TES | Thermal Energy Storage |
| WTF | Working Transfer Fluid |

*Greek Symbols*

| | |
|---|---|
| $\alpha$ | Convective Heat Transfer Coefficient |
| $\Delta$ | Pressure drop |
| $\eta$ | Efficiency |
| $\rho$ | Density |

*Subscripts*

| | |
|---|---|
| e | electrical |
| g | gas |
| i | internal |
| p | particles |
| th | thermal |

## References


[1] K. Lovegrove, W. Stein, Concentrating Solar Power Technology: Principles, Developments and Applications, Woodhead Publishing, 2012.
[2] H.L. Zhang, J. Baeyens, J. Degrève, G. Cacères, Concentrated solar power plants: review and design methodology, Renew. Sustain. Energy Rev. 22 (2013) 466–481, https://doi.org/10.1016/j.rser.2013.01.032.
[3] C.S.P. Alliance, The Economic and Reliability Benefits of CSP with Thermal Energy Storage: Recent Studies and Research Needs, 2014, https://doi.org/10.1017/CBO9781107415324.004.
[4] H. Martín, J. de la Hoz, G. Velasco, M. Castilla, J.L. García de Vicuña, Promotion of concentrating solar thermal power (CSP) in Spain: performance analysis of the period 1998–2013, Renew. Sustain. Energy Rev. 50 (2015) 1052–1068, https://doi.org/10.1016/j.rser.2015.05.062.
[5] SunShot initiative, US Department of Energy, 2015. http://energy.gov/eere/sunshot/sunshot-initiative.
[6] STAGE-STE EERA, Scientific and Technological Alliance for Guaranteeing the European Excellence in Concentrating Solar Thermal Energy, 2013. http://www.stage-ste.eu/.
[7] A.T. Kearney GmbH, Solar Thermal Electricity 2025. Clean Electricity on Demand: Attractive STE Cost Stabilize Energy Production. Dusseldorf, 2010.
[8] M.A. Reyes-Belmonte, A. Sebastián, J. González-Aguilar, M. Romero, Performance comparison of different thermodynamic cycles for an innovative central receiver solar power plant, in: AIP Conference Proceedings, Vol. 1850, AIP Publishing LLC, 2017, p. 160024, https://doi.org/10.1063/1.4984558.
[9] M.A. Silva-Perez, Solar Power Towers Using Supercritical CO2 and Supercritical Steam Cycles, and Decoupled Combined Cycles, Elsevier Ltd, 2016, https://doi.org/10.1016/B978-0-08-100516-3.00017-4.
[10] S. Giuliano, R. Buck, S. Eguiguren, Analysis of solar-thermal power plants with thermal energy storage and solar-hybrid operation strategy, J. Sol. Energy Eng. 133 (2011) 1–8, https://doi.org/10.1115/1.
[11] C.S. Turchi, Z. Ma, T.W. Neises, M.J. Wagner, Thermodynamic study of advanced supercritical carbon dioxide power cycles for concentrating solar power systems, J. Sol. Energy Eng. 135 (2013) 041007, https://doi.org/10.1115/1.4024030.
[12] M.A. Reyes-Belmonte, A. Sebastián, M. Romero, J. González-Aguilar, Optimization of a recompression supercritical carbon dioxide cycle for an innovative central receiver solar power plant, Energy 112 (2016) 17–27, https://doi.org/10.1016/j.energy.2016.06.013.
[13] G. Flamant, D. Gauthier, H. Benoit, J.-L. Sans, R. Garcia, B. Boissière, et al., Dense suspension of solid particles as a new heat transfer fluid for concentrated solar thermal plants: on-sun proof of concept, Chem. Eng. Sci. 102 (2013) 567–576, https://doi.org/10.1016/j.ces.2013.08.051.
[14] H. Benoit, I.P. López, D. Gauthier, G. Flamant, Temperature influence on wall-to-particle suspension heat transfer in a solar tubular receiver, Solar Paces 1734 (2015) 040002, https://doi.org/10.1063/1.4949093.
[15] C.K. Ho, S.S. Khalsa, N.P. Siegel, Modeling on-sun tests of a prototype solid particle receiver for concentrating solar power processes and storage, in: ASME 2009 3rd International Conference on Energy Sustainability, vol. 2, ASME, 2009, pp. 543–550, https://doi.org/10.1115/ES2009-90035.
[16] D. Geldart, Types of gas fluidization, Powder Technol. 7 (1973) 285–292, https://doi.org/10.1016/0032-5910(73)80037-3.
[17] H. Benoit, Recepteur Solaire Tubulaire a Suspension Dense de Particules en Ecoulement Ascendant. Université de Perpignan, 2015.
[18] Y. Zhu, R. Zhai, J. Qi, Y. Yang, M.A. Reyes-Belmonte, M. Romero, et al., Annual performance of solar tower aided coal-fired power generation system, Energy (2016), https://doi.org/10.1016/j.energy.2016.11.023.
[19] M. Puppe, S. Giuliano, M. Krüger, O. Lammel, R. Buck, S. Boje, et al., Hybrid high solar share gas turbine systems with innovative gas turbine cycles, Energy Procedia (2015), https://doi.org/10.1016/j.egypro.2015.03.129.
[20] A. Rovira, C. Sánchez, M. Valdés, R. Abbas, R. Barbero, M. Montes, et al., Comparison of different technologies for integrated solar combined cycles: analysis of concentrating technology and solar integration, Energies 11 (2018) 1064, https://doi.org/10.3390/en11051064.
[21] G. Polonsky, M. Livshits, A.I. Selwynraj, S. Iniyan, L. Suganthi, A. Kribus, Annual performance of the solar hybrid STIG cycle, Sol. Energy 107 (2014) 278–291, https://doi.org/10.1016/j.solener.2014.05.022.
[22] Y. Touloukian, Thermophysical Properties of High Temperature Solid Materials, Macmillan, New York, 1967.
[23] CSP2, Concentrated Solar Power in Particles, European Comission, 2013. http://www.csp2-project.eu/.
[24] G. Flamant, D. Gauthier, H. Benoit, J.-L. Sans, B. Boissière, R. Ansart, et al., A new heat transfer fluid for concentrating solar systems: particle flow in tubes, Energy Procedia 49 (2014) 617–626, https://doi.org/10.1016/j.egypro.2014.03.067.
[25] H. Benoit, I. Pérez López, D. Gauthier, J.-L. Sans, G. Flamant, On-sun demonstration of a 750°C heat transfer fluid for concentrating solar systems: dense particle suspension in tube, Sol. Energy 118 (2015) 622–633, https://doi.org/10.1016/j.solener.2015.06.007.
[26] MathWorks – Makers of MATLAB and Simulink - MathWorks España n.d. http://www.mathworks.com/.
[27] J. Spelling, Hybrid Solar Gas-Turbine Power Plants - a Thermoeconomic Analysis, 2013.
[28] TRNSYS, Transient System Simulation Tool 2016. http://www.trnsys.com/. (Accessed 20 January 2016).
[29] P. Schwarzbözl, A TRNSYS Model Library for Solar Thermal Electric Components ( STEC ) Reference Manual, 2006.
[30] WinDelsol 1.0 Users Guide, 2002.
[31] M.A. Reyes-Belmonte, F. Gómez-García, J. González-Aguilar, M. Romero, H. Benoit, G. Flamant, Heat exchanger modelling in central receiver solar power plant using dense particle suspension, in: AIP Conference Proceedings, Vol. 1850, AIP Publishing LLC, 2017, p. 030042, https://doi.org/10.1063/1.4984385.
[32] B.L. Kistler, A User's Manual for DELSOL3: a Computer Code for Calculating the Optical Performance and Optimal System Design for Solar Thermal Central Receiver Plants, 1986.
[33] A. Gallo, J. Spelling, M. Romero, J. González-Aguilar, Preliminary design and performance analysis of a multi-megawatt scale dense particle suspension receiver, Energy Procedia 69 (2015) 388–397, https://doi.org/10.1016/j.egypro.2015.03.045.
[34] F. Gomez-Garcia, D. Gauthier, G. Flamant, Design and performance of a multistage fluidised bed heat exchanger for particle-receiver solar power plants with storage, Appl. Energy 190 (2017) 510–523, https://doi.org/10.1016/j.apenergy.2016.12.140.
[35] P. Steiner, K. Schwaiger, H. Walter, Active fluidized bed technology used for thermal energy storage, in: Proceedings of the ASME 2016 10th International Conference on Energy Sustainability, ASME, Charlotte, North Carolina, 2016, pp. 1–10.
[36] K. Schwaiger, M. Haider, M. Hämmerle, D. Wünsch, M. Obermaier, M. Beck, et al., SandTES - an active thermal energy storage system based on the fluidization of powders, Energy Procedia 49 (2013) 983–992, https://doi.org/10.1016/j.egypro.2014.03.106.
[37] B. Sakadjian, S. Hu, M. Maryamchik, T. Flynn, K. Santelmann, Z. Ma, Fluidized-bed technology enabling the integration of high temperature solar receiver CSP systems with steam and advanced power cycles, Energy Procedia 69 (2015) 1404–1411, https://doi.org/10.1016/j.egypro.2015.03.126.
[38] P.H. Wagner, M. Wittmann, Influence of different operation strategies on transient solar thermal power plant simulation models with molten salt as heat transfer fluid, Energy Procedia 49 (2014) 1652–1663, https://doi.org/10.1016/j.egypro.2014.03.174.
[39] M. Wittmann, M. Eck, R. Pitz-Paal, H. Müller-Steinhagen, Methodology for optimized operation strategies of solar thermal power plants with integrated heat storage, Sol. Energy 85 (2011) 653–659, https://doi.org/10.1016/j.solener.2010.11.024.
[40] S. Kuravi, J. Trahan, D.Y. Goswami, M.M. Rahman, E.K. Stefanakos, Thermal energy storage technologies and systems for concentrating solar power plants, Prog. Energy Combust. Sci. 39 (2013) 285–319, https://doi.org/10.1016/j.pecs.2013.02.001.
[41] R. Guédez, J. Spelling, B. Laumert, T. Fransson, Optimization of thermal energy storage integration strategies for peak power production by concentrating solar power plants, Energy Procedia (2014), https://doi.org/10.1016/j.egypro.2014.03.173.
[42] E. Casati, F. Casella, P. Colonna, Design of CSP plants with optimally operated thermal storage, Sol. Energy 116 (2015) 371–387, https://doi.org/10.1016/j.solener.2015.03.048.
[43] G. Augsburger, Thermo-economic Optimisation of Large Solar Tower Power Plants PAR, 2013, p. 253, https://doi.org/10.5075/epfl-thesis-5648, 5648.
[44] J. Edman, J. Windahl, Dynamic modeling of a central receiver CSP system in modelica, in: Proceedings of the 11th International Modelica Conference, 2015, pp. 585–594, https://doi.org/10.3384/ecp15118585.
[45] L.F. Drbal, P. Boston, K. Westra, B. Erickson, Power Plant Engineering, Springer, 1996.
[46] K. Schwaiger, M. Haider, Design of a utility scale solar thermal tower system based on particle receivers and fluidized bed technology, in: SASEC2015 Third Southern African Solar Energy Conference, Kruger National Park, South Africa, 2015.
[47] Meteonorm 7.1.10: Irradiation Data for Every Place on Earth n.d. http://www.meteonorm.com/.
[48] Q. Kang, R. Dewil, J. Degrève, J. Baeyens, H. Zhang, Energy analysis of a particle suspension solar combined cycle power plant, Energy Convers. Manag. 163 (2018) 292–303, https://doi.org/10.1016/J.ENCONMAN.2018.02.067.
[49] H. Zhang, H. Benoit, I. Perez-Lopèz, G. Flamant, T. Tan, J. Baeyens, High-efficiency solar power towers using particle suspensions as heat Carrier in the receiver and in the thermal energy storage, Renew. Energy 111 (2017) 438–446, https://doi.org/10.1016/J.RENENE.2017.03.101.
[50] J. Spelling, A. Gallo, M. Romero, J. González-Aguilar, A high-efficiency solar thermal power plant using a dense particle suspension as the heat transfer fluid, Energy Procedia 69 (2015) 1160–1170, https://doi.org/10.1016/j.egypro.2015.03.191.